IOP Publishing Phys. Med. Biol. 64 (2019) 185018 (12pp) https://doi.org/10.1088/1361-6560/ab18b3

Physics in Medicine & Biology

IPEM Institute of Physics and Engineering in Medicine

OPEN ACCESS

PAPER

Towards a metamaterial approach for fast timing in PET: experimental proof-of-concept

R M Turtos[1,2,3], S Gundacker[1,2], E Auffray[1,2] and P Lecoq[1,2]

[1] CERN, Geneva 23, 1211, Switzerland
[2] Universita degli Studi di Milano-Bicocca, Piazza dell'Ateneo Nuovo 1, 20126 Milano, Italy
[3] Author to whom any correspondence should be addressed.

E-mail: rosana.martinez.turtos@cern.ch

Keywords: fast timing, scintillators-based detectors, TOF-PET

RECEIVED
20 December 2018

REVISED
15 March 2019

ACCEPTED FOR PUBLICATION
12 April 2019

PUBLISHED
19 September 2019

Abstract

Achieving fast timing in positron emission tomography (PET) at the level of few tens of picoseconds of picoseconds is limited by the photon emission rate of existent materials with standard scintillation mechanisms. This has led to consider quantum confined excitonic sub-1 ns emission in semiconductors as a viable solution to enhance the amount of fast-emitted photons produced per gamma event. However the introduction of nanocrystals and nanostructures into the domain of radiation detectors is a challenging problem. In order to move forward along this line, the standard bulk detector geometry and readout should be updated to allow for the implementation of new materials and within others, compensate for some of their intrinsic limitations. In this paper we will cover two study cases in which a fast emitter is combined with state-of-the-art scintillators in a sampling geometry designed to provide better timing for a fraction of the 511 keV events. For this test, we use a fast plastic scintillator BC-422 able to deliver a detector time resolution (DTR) of 25 ps FWHM (equivalent coincidence time resolution CTR of 35 ps) and we combined it with LYSO or BGO 200 μm thick plates building a sampling pixel composed by two active scintillating materials. We develop a new proof of concept readout that allows for the identification of different types of events, carrying standard or improved timing information. Results are showing a DTR of 67 ps FWHM (equivalent to a CTR of 95 ps) for one third of the events depositing 511 keV in the BGO + BC-422 $3.8 \times 3.8 \times 3$ mm^3 sampling pixel. The other two third of the 511 keV events perform like standard bulk 3 mm long BGO crystals with a time resolution of around 117 ps (equivalent to a CTR of 165 ps). For the case of LYSO + BC-422 sampling pixel, shared 511 keV events reach a DTR of 39 ps (CTR of 55 ps) in comparison to 57 ps (CTR of 83 ps) for 511 keV events fully contained in LYSO of the same size. This work is a step forward in the integration of fast semiconductor nanocrystals and nanostructures with present detector technologies.

1. Introduction

Pushing the timing resolution of radiation detectors to the 10 ps level faces major technological challenges, especially in the low energetic regime of few hundred keV. If achieved, reaching the mentioned timing in scintillator-based calorimeters would highly impact particle tracking algorithms and image reconstruction techniques, both in high energy physics and positron-emission-tomography (Lecoq 2017). Challenges are in short mostly driven by two main factors. First, the scintillation emission rate of existing materials and second the single photon time resolution (SPTR) of state-of-the-art photodetectors and associated readout electronics (Gundacker *et al* 2016b). If we look into the photostatistic of state-of-the-art scintillators like LYSO for example, the best performing material is able to emit around one photon per MeV per picosecond, which limits the amount of information available in the first 10 ps after a 511 keV gamma has been detected. Moreover, the fact that we use the scintillator as a waveguide to transport isotropically emitted light reduces the number and smears the timing of the first photons. Hence, light emission and transport constitute nowadays the main bottlenecks to achieve ultrafast timing with moderate energies and standard scintillators. Therefore, in this contribution we focus our

attention in materials able to overcome the limitations associated to low photon time density and we propose a feasible approach in order to implement them as radiation detectors.

Materials with a very sharp scintillating response in the sub-1 ns regime have been previously studied (Padilha *et al* 2013, Turtos *et al* 2016a) and they are found in the form of semiconductor nanoplatelets (Turtos *et al* 2016c) or multiple quantum well heterostructures (Hospodková *et al* 2017). In this case the quantum confinement of electron-hole pairs plays a significant role in enhancing the matrix element for the radiative transition (Wilkinson *et al* 2004) and it is also responsible for one of the most interesting features of scintillating nanocrystals: biexcitons with a very high binding energy and therefore stable at room temperature (Grim *et al* 2014). Moreover, the 1D confinement contributes to the red-shifted emission of such biexcitons which helps to enlarge the small Stokes-shift characteristic of direct band gap semiconductors. Unfortunately, the use of these materials in the ionizing radiation detector field is constraint by numerous reasons. First, their very small size intrinsically limits the amount of energy that can be deposited in individual nanoparticles (Bulin *et al* 2015) and increases the probability of non-radiative channels (Kharchenko and Rosen 1996, Klimov 2014), charging effects, etc. Second, they are usually direct band-gap semiconductors presenting very high self-absorption. Third, their overall effective density and stopping power is rather limited due to either low effective atomic number Z, low packing fraction or insufficient achievable thickness determined by current nano-fabrication techniques. To make a practical use of these new materials, a different detector configuration should be employed such that the nanocrystals can perform as time taggers, whereas high-Z scintillators take the role of stopping the ionizing radiation.

For the time being we will focus our effort in optimizing timing when detecting 511 keV gammas due to the envisioned impact that this could bring to the medical imaging community and the time-of-flight positron emission tomography (TOF-PET) technique (Lecoq 2017). Thus, we are placing this research in the frame of the 10 ps TOF-PET challenge.

In this contribution we put in practice a new detector configuration for the purpose of improving the scintillator's time resolution based on a sampling pixel geometry. This novel arrangement combines thin layers of a high-Z inorganic scintillator, bringing a high stopping power and photoelectric probability, with a light plastic scintillator presenting a much faster photoemission. Each high-Z layer has a thickness determined by the range of the recoil electron produced upon a photoelectric absorption, which for the case of LYSO and BGO is about 200 μm. In between the dense scintillating layers, we include plates of a fast and unfortunately light scintillating material, which contributes to increase the overall photon-time-density for the fraction of the events able to share energy between both materials. This work serves as a follow-up of previous studies in Gundacker *et al* (2016b), where prompt photons are artificially added on top of the standard scintillating signal as the strategy to reach 10 ps coincidence time resolution (CTR). A schematic representation of the basic idea at the center of this paper is shown in figure 1.

For the first exploratory studies we use a fast plastic BC-422 scintillator combined with LYSO or BGO plates to make a proof of concept for new readout techniques. The energy distribution of 511 keV gammas have been estimated using Geant4, a Monte Carlo-based particle tracking algorithm. The simulation of the system allows to calculate a feasible sampling thickness for the construction of the hybrid pixel able to provide a substantial number of events carrying better timing information. For a sampling thickness of about 200 μm, the number of 511 keV events able to fully deposit their energy among both materials represents around one third of the total. This factor, even though when is not optimal, gives a starting point to understand and identify the different types of events present in a sampling pixel. Two $3.8 \times 3.8 \times 3$ mm^3 sampling pixels were assembled, a first one composed by alternating 200 μm thick plates of BGO with 250 μm plates of BC-422 and a second one using LYSO plates instead. The experimental readout has three main objectives: 1. to identify the events depositing their energy in one or both materials, i.e. normal or shared events, 2. to differentiate Compton normal or shared events from 511 keV normal or shared events and 3. characterize the time resolution given by 511 keV events, shared or not shared.

Our goal is to show that a sampling approach of the scintillating pixel is able to improve timing for a fraction of the events sharing 511 keV.

2. Materials and methods

2.1. BC-422 combined with BGO or LYSO for a proof-of-concept readout

To develop the single channel readout of a scintillating pixel with two active materials we have chosen the plastic BC-422 scintillator from Saint-Gobain (2016) due to its fast photon emission characteristics. This plastic presents a rise time of around 30 ps and a decay time of 1.26 ns for 80% of the total emission (7.2 ns for 20%) measured with a time-correlated single photon counting setup (TCSPC) with 511 keV excitation (Gundacker *et al* 2016b). The light yield reported is around 10 000 ph MeV^{-1} which has been confirmed by comparing to the light output of bulk LYSO $3 \times 3 \times 3$ mm^3 measured under the same dry coupling and ESR reflector (Vikuiti) wrapping conditions. BC-422 plates with a thickness of about 250 μm were prepared and cut in our workshop at CERN

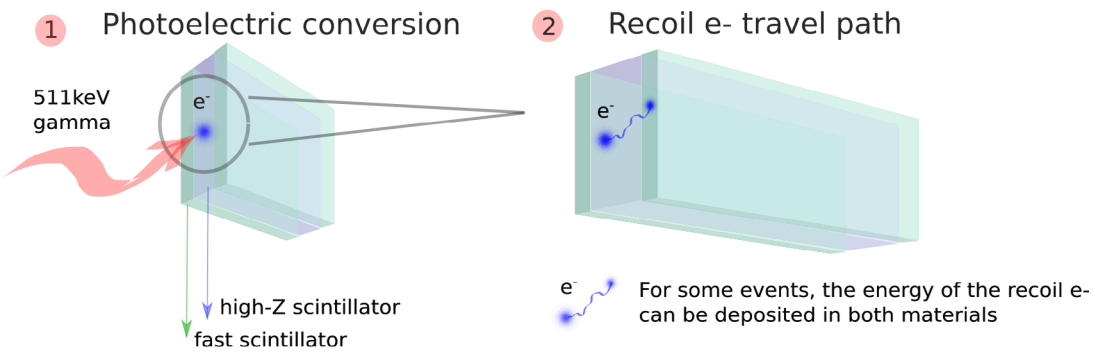

Figure 1. 511 keV gamma interacting with a sampling pixel.

without the possibility of polishing the long 3×3 mm^2 faces. Therefore, sampling pixels were assembled with unpolished BC-422 plates. The photostatistic of the BC-422 plastic scintillator combined with high frequency electronic readout and improved photodetectors from FBK with a SPTR of 70 ps FWHM (Gundacker *et al* 2019) yield a CTR of 35 ps FWHM for events selected to the 340 keV Compton edge. Therefore, it constitutes a good candidate to make a proof-of-concept for this study.

The LYSO used in this contribution is in the shape of tiles and it has been combined with BC-422 to form a pixel with a total volume of $3.8 \times 3.8 \times 3$ mm^3. Each sampling pixel is composed of eight plates of high-Z material and 7–8 plates of BC-422 as shown in figure 2. The LYSO tiles were produced by CPI with a size of $3 \times 3 \times 0.2$ mm^3 and the two large faces polished. The light output test using 10 LYSO tiles separated by an air gap under the same coupling and wrapping conditions shows a slight energy resolution deterioration going from 11% (no grease coupling) to 13% with a loss in light output of also around 13% as compared to bulk LYSO. The time resolution of bulk $3 \times 3 \times 3$ mm^3 LYSO:Ce from CPI measured with the same SiPM and high frequency electronic (Gundacker *et al* 2019) is 54 ps FWHM (equivalent CTR of 76 ps).

The other scintillator used in this study is bismuth germanate $Bi_4Ge_3O_{12}$. BGO stands out due to its high photo-fraction and has been the standard scintillator used in PET for many years. However it was substituted by LSO in time-of-flight scanners due to its limited timing performance. BGO presents a lower light yield of around 8000–9000 ph MeV^{-1} and longer decay time of 300 ns approximately. Recent developments using high frequency electronic readout are able to lower the DTR of this crystal to 112 ps FWHM (equivalent CTR of 158 ps) by exploiting Cherenkov photons in a short 3 mm long crystal (Gundacker *et al* 2019). For this study, we use BGO plates 3×3 mm^2 in area and 200 μm thick produced by EPIC with the two large faces polished. The sampling pixel composed by BGO and BC-422 is built by combining BGO plates $3 \times 3 \times 0.2$ mm^3 with two large faces polished and BC-422 plates $3 \times 3 \times 0.25$ mm^3 with the two large faces unpolished, as shown on the right-hand side of figure 2.

For the first studies and in order to minimize light sharing between the different materials, we used an air gap in-between the plates and we placed them by alternating different materials in a 3D-printed $3.8 \times 3.8 \times 3$ mm^3 holder with the walls covered by ESR reflector Vikuiti. The light transport within the BC-422 plates is rather complex due to the unpolished large faces and the smaller index of refraction. However, as confirmed by light output measurements, the high-Z plates conserve the total-internal-reflection driven light transport within individual plates.

A summary of the main scintillating characteristics presented by BC-422, LYSO and BGO in their block form of a $3 \times 3 \times 3$ mm^3 cube is shown in table 1.

2.2. Geant4-based Monte Carlo simulations of energy deposited in a sampling pixel

Geant4 simulations (Turtos *et al* 2016b) were used to estimate the fraction of events providing better timing or in other words the fraction of shared events with full energy deposition. The tracking of 511 keV gammas have been validated using very well-known configurations as those of bulk homogeneous materials like LYSO or BGO 3 mm long. For the homogeneous case, the attenuation length of each material for 511 keV gammas (12 mm for LYSO and 11 mm for BGO) allows to calculate the percentage of detected events, which should follow the formula $1\text{-}I/I_o = 1 - e^{-\frac{x}{\mu_l}}$. Both, detection efficiency and photofraction are well predicted when simulating bulk LYSO or BGO 3 mm long, which is the length employed for this study.

Simulations are set-up by reproducing the sampling pixel geometry presented in section 2.1 and tracking 511 keV gammas and their secondary particles as they travel and deposit energy through the different materials, step by step. The Physics list used is the Standard Electromagnetic list and each material is treated as two different detector classes. The classification of events is determined by the total energy deposited in the sampling pixel as a

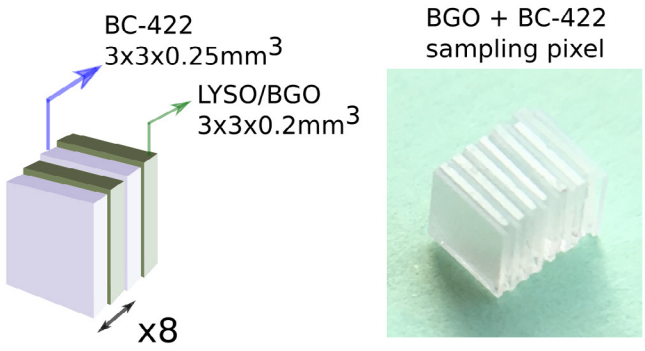

Figure 2. Schematics and picture of the sampling pixels components.

Table 1. Scintillating characteristics of BC-422, LYSO and BGO block crystals and associated DTR.

Scint	τ_r^a (ps)	τ_d^a (A%) (ns)	LO[b] (ph MeV^{-1})	E$_R^c$ (%)	DTR[d] (ps)	ρ (g cm^{-3})
BC-422	30	1.26 (80%)	9000	—	25	1.03
LYSO	50	40 (100%)	27 000	9%	54	7.1–7.3
BGO	Cherenkov	351 (94%)	6300	13%	112	7.13

[a] Measurements taken with a time correlated single photon counting setup reported in Gundacker *et al* (2016b) with IRF of 63 ps sigma.
[b] Light output measurements taken with 3 × 3 × 3 mm^3 homogeneous cubes using Teflon wrapping and grease coupling. The values are normalized to results reported in Gundacker *et al* (2016a) for LYSO:Ce CPI 3 × 3 × 3 mm^3.
[c] Values reported taking into account background, Compton edge and a Gaussian fit for the x-ray escape and photoelectric peaks.
[d] DTR measurements taken with a coincidence setup reported in Gundacker *et al* (2019).

whole. Energy is added up step by step and summed at the end of the event taking into account in which material the energy was deposited. Events with partially deposited energy, i.e. final sum smaller than 511 keV, are going to be labeled as 'Compton events'. On the other hand, events that origin from a photoelectric absorption or a Compton interaction in the high-Z material or the plastic, and the sum of energy deposited in both materials equals 511 keV will be labeled as '511 keV'. A further classification, separates 511 keV labeled events as normal or shared, whether the energy was deposited in one or both materials, respectively. From these two types of 511 keV events, the ones not able to leak energy out of the high-Z plate (normal) and the ones who do (shared), we expect a different timing performance.

Normal events will carry the timing provided by the photostatistic of the high-Z scintillator. Shared events, in dependence of the energy distribution between both materials, would provide a better timing due to the contribution from the fast emitter. As expected, the percentage of events with improved timing with respect to the total number of gammas detected and events depositing 511 keV is highly dependent on the sampling thickness and the density of both materials.

2.3. Coincidence time resolution bench

For the timing readout, we have coupled the sampling pixel to a 4 × 4 mm^2 FBK NUV-HD SiPM 40 μm SPAD size and placed it in coincidence with an LSO:Ce:Ca co-doped 2 × 2 × 3 mm^3 crystal as shown in figure 3. The measurements were performed by coupling the plates perpendicularly to the SiPM so that light can be channeled through the individual plates for the high-Z scintillator as displayed in figure 3(a). The bench in use is an upgraded version of the one reported in Gundacker *et al* (2016a). It is light-tight and temperature controlled at 15 ± 0.1 °C. The ^{22}Na source in use had an activity of 756 kBq in 2015.

The SiPM electronics readout for the reference detector was done, as usual, based on two amplifiers from which we obtain the energy and time stamps separately (left hand-side of figure 3(a)). However for this specific case, the time stamps are obtained with a high-frequency amplifier having a bandwidth of around 1.5 GHz as reported in Gundacker *et al* (2019). The CTR of the reference detector in use is 58 ps FWHM. This value has been obtained by measuring two LSO:Ce:Ca 2 × 2 × 3 mm^3 crystals in coincidence using two FBK NUV-HD SiPMs as photodetectors. The SPAD size of the SiPMs used was 40 μm with a measured SPTR of 70 ps FWHM at a bias voltage of 39 V (10.8 V over breakdown). Data is analyzed with a Lecroy DDA735Zi oscilloscope, 3.5 GHz bandwidth and a sampling rate of 40 Gs s^{-1} (using four channels this reduces to 20 Gs s^{-1}, i.e. 50 ps binning). These and other technicalities of the setup are explained in more details in Gundacker *et al* (2019).

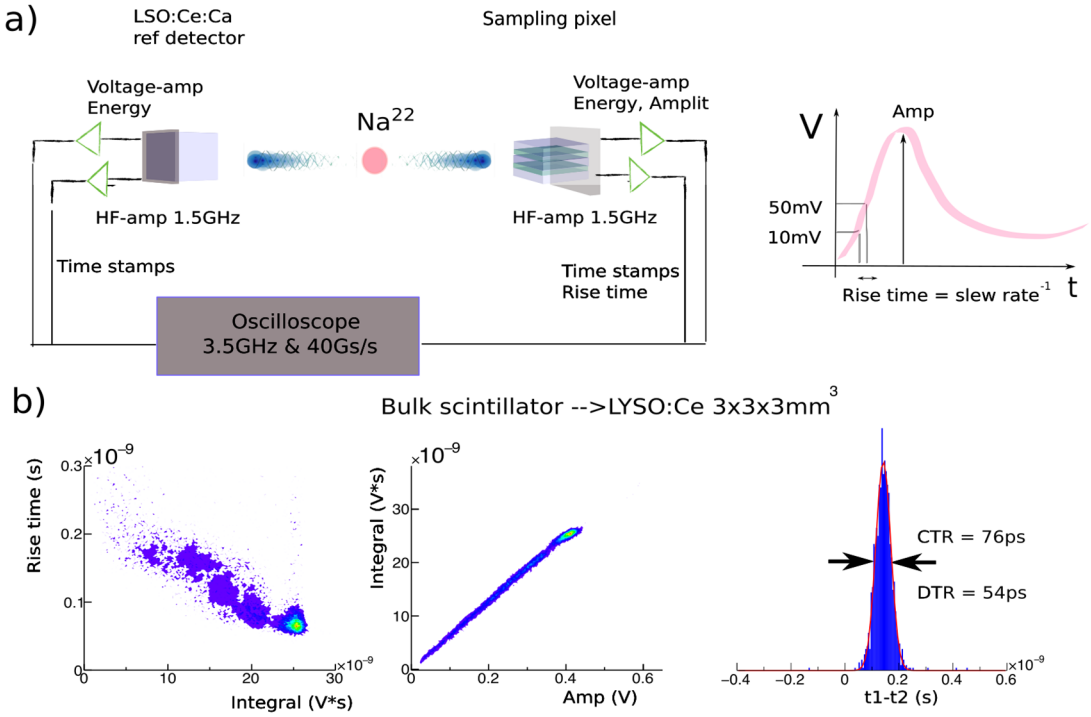

Figure 3. (a) CTR setup used for the single channel readout of sampling scintillating pixels. Together with the integral and time at the leading edge threshold, the amplitude and the rise time of the signal are also measured. (b) Anti-correlation between rise time and integral (left) and correlation between amplitude and integral (center) measured for the standard case of one bulk scintillating crystal. Right: CTR obtained for LYSO:Ce bulk 3 mm cubic crystal using high-frequency readout. The amplitude of a single cell is 44 mV (Gundacker *et al* 2019).

For these studies, we are interested in the timing performance of the single sampling pixel, i.e. the DTR. If two similar detectors would be used, the DTR can be calculated dividing the CTR by $\sqrt{2}$. Hence the reference detector has a DTR of 41 ps.

For the readout of the sampling pixels (right of the Na^{22} source) we investigated how the amplitude, integral and rise time correlate with each other in order to identify the different categories of events. Regarding energy, both integral and amplitude of the signal are measured using the voltage amplifier. For the timing, we make use of the high frequency amplifier which allows to register the leading edge time at very low thresholds and measure fast signal rise times between 10 and 50 mV in this particular setup. This is shown in the schematics of figure 3(a). As an example, figure 3(b) shows the two types of correlations used in this study, i.e. rise time versus integral and integral versus amplitude and how they would appear for the standard case of LYSO:Ce scintillators. The rise time of the signal is anti-correlated to the integral meanwhile the amplitude and the integral will show a linear correlation. The data presented in figure 3(b) were taken with an LYSO:Ce $3 \times 3 \times 3$ mm^3 from the same producer (CPI) that manufactured the plates used in the sampling pixel. The distribution of time stamps is fitted to a Gaussian function, from which the standard deviation and the FWHM is obtained.

In contrast to LYSO, BGO has been chosen due to its excellent photofraction, its slower decay time and smaller light yield. Basically, its pulse shape determined by rise time, amplitude and integrated charge differs very much from BC-422 and this allows to identify the different types of events more easily, making use of the two extra parameters, amplitude and rise time. It is worth noticing that the rise time used in this contribution, i.e. inverse of the signal slew rate between 10 and 50 mV, is actually a parameter for the immediate photostatistic and not by any means the scintillation rise time. For the specific case of the BGO + BC-422 sampling pixel, was coupled to the SiPM using Meltmount glue (index of refraction 1.68) with a near UV transmission cut-off that overlaps with the emission from the plastic, centered at 370 nm, so we might not be able to extract very efficiently near UV photons in this configuration. On the other hand, the measurements of the LYSO + BC-422 pixel were done after coupling with Meltmount, index of refraction 1.58, having a transmission close 80% at 370 nm instead of around 50% as for the $n = 1.68$ Meltmount.

3. Results

3.1. Simulations of 511 keV gammas detected by a sampling pixel

In this section, we present the results obtained after tracking 511 keV gammas using the sampling pixels as detectors. One of the main concerns regarding the use of plastic scintillators for PET is based on its low density, hence low stopping power. Indeed, the overall detection efficiency of the new pixelated configurations decreases

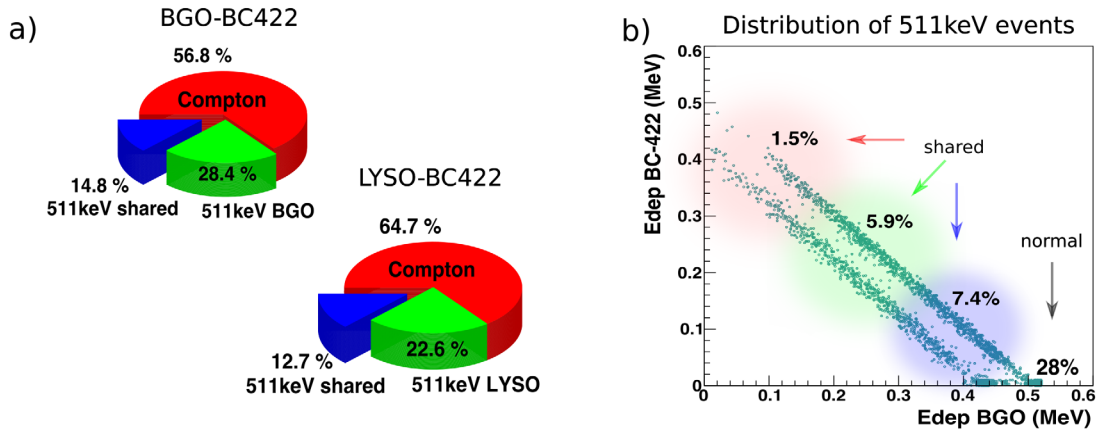

Figure 4. Energy distribution map for 511 keV gammas detected by BGO/LYSO + BC-422 sampling pixels (a). The pie chart shows the percentage of the different categories of events with respect to the total number of gammas detected. (b) Energy deposited in BGO versus energy deposited in BC-422 in the sampling pixel. For visualization purposes Compton events have been removed from the 2D plot.

from 24% for the case of BGO 3 mm long down to around 14% for a sampling pixel containing 200 μm BGO plates and 250 μm BC-422 plates. A similar situation appears when exchanging BGO by LYSO, in this case the detection efficiency decreases from 22% down to around 12%. Comparing BGO + BC-422 to bulk LYSO, we reach around 60% stopping efficiency without further optimization.

The distribution of how the energy is shared between the two scintillating materials for both BGO + BC-422 and LYSO + BC-422 pixels is shown in figure 4(a). We can observe how the 511 keV gamma is roughly two out of three times fully contained in the BGO/LYSO plates, which yields events with the standard BGO/LYSO timing. However for one third of the 511 keV events fully deposited in the sampling pixel, the energy is shared between the two scintillators. The main difference between LYSO and BGO sampling pixels is due to its higher photofraction which decreases the number of 'Compton events' for the BGO-based sampling pixel.

Looking at the distribution of energy within the 'shared 511 keV events' in figure 4(b), we count around 50% of the shared events with most of the energy deposited in BGO and leaking less than 100 keV to the plastic. The other 50% of the events are composed by those depositing at least around 250 keV in BC-422 and a minority of the events depositing more than 300 keV in plastic. This distribution of energy introduces an amplitude fluctuation in the signal due to the variable number of fast photons for each event. Thus, a bias correction in the form of time-walk needs to be applied to the final time distributions. The distribution of shared 511 keV events for the case of LYSO + BC-422 follows the same trend due to the very similar density.

3.2. Timing with the BGO + BC-422 sampling pixel

The assembly of the pixel follows the geometry mentioned in previous sections, 200 μm thick BGO tiles and alternated BC-422 250 μm thick plates with an air gap in-between plates. The ensemble of around 15 plates in total are hold by a 3D printed cube, which has all five walls covered by the ESR reflector, Vikuiti. The pixel is coupled to a FBK NUV-HD SiPM using Meltmount with index of refraction of 1.68 and with the high aspect-ratio surface of the plates (3×0.2 mm^2) facing the photodetector. The readout is similar to that of a standard CTR measurement, except that we use two extra parameters in order to identify the different categories of events. In addition to integrated charge, i.e. energy, we record the rise time and the amplitude of the signal.

The data obtained when measuring the BGO + BC-422 sampling pixel in coincidence with the LSO:Ce:Ca co-doped reference crystal is shown in figure 5. Measurements were taken using a 200 ns integration gate, which allows to collect around 50% of the BGO scintillation emission and close to 100% for the BC-422. However, the different emission spectra might yield different extraction efficiencies due to the Meltmount used. A threshold scan has been implemented, starting from 1mV up to 80mV. Results presented here are taken for a particular run where the threshold is fixed to 10mV yielding best timing results.

The integral of the signal has been plotted against the rise time as shown in figure 5(a). This allows to distinguish gammas fully contained in BGO by choosing events with a rise time higher than 100 ps. The rest of the events exhibiting a faster rise time would be events depositing energy in plastic either shared or not. Looking at the correlation plot of integral versus amplitude shown in figure 5(b), we are able to identify three main areas: 1. events fully contained in BGO which represents around 70% of the events, 2. events fully contained in BC-422 and 3. 511 keV shared events. Basically all the events showing up in-between the lines which define BGO and BC-422 are events sharing energy between these two materials. The events with full energy deposition will extend from the photopeak of the high-Z material towards the photopeak channel of the plastic, i.e. integrated charge

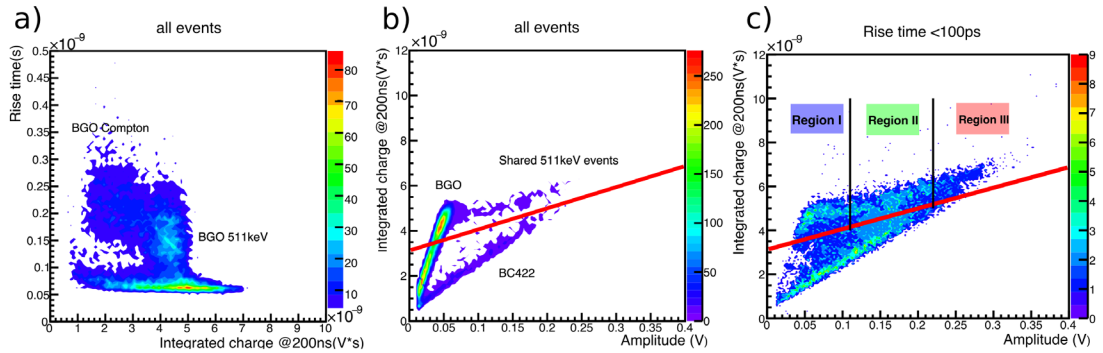

Figure 5. Event identification for the BGO + BC-422 sampling pixel. (a) Rise time as function of the integral for all the events in coincidence. (b) Integral as a function of the amplitude for all the events in coincidence. (c) Integral as a function of the amplitude for the events with a rise time smaller than 100 ps.

or amplitude higher than those corresponding to the plastic Compton edge. Figure 5(c) shows how the integral correlates with the amplitude for all events that are not fully contained in BGO. For this, we have taken the plot shown in (b) and we have applied a cut based on the rise time of the signal, so we are basically looking at the events with a rise time smaller than 100 ps.

Following our analysis, the time resolution along the line of events which corresponds to 511 keV shared energy, should improve for those events with a larger contribution from the BC-422, i.e. higher amplitude. The more light emitted from BC-422, the higher the amplitude of the signal. Actually, we are able to observe the Compton edge from events depositing energy only in the BC-422 plastic with an integral of around 4 nVs and an amplitude of 200 mV. Values higher than those in terms of integral or amplitude are shared events with an overall energy deposited higher than 340 keV.

We can separate the line of events corresponding to 511 keV shared energy into three different regions (figure 5(c)). Region I has an integral close to values seen when 511 keV is solely deposited in BGO but higher amplitude and faster rise time. This indicates that 511 keV have deposited most of the energy in BGO and the rest goes to the plastic. Region III would be the opposite, most of the energy have been deposited in the plastic, i.e. 340 keV and the rest is leaking out to BGO. Finally, region II would be in-between, so the energy is deposited approximately even in both materials. The three regions have been chosen very coarsely cause the energy calibration of the setup has not been performed. We can not therefore correct by saturation issues in the SiPM but we are able to observe when 511 keV shared events have higher amplitudes than the Compton edge of the BC-422 plastic. This Compton edge is placed around 4 nVs in the integral axis and 200 mV in the amplitude axis, so Region III corresponds to events with an amplitude higher than the Compton edge in plastic, i.e. energy in the plastic higher than 340 keV. For Region I and II, we divide the range half way.

Figure 6(a) shows the time walk influence of 511 keV shared events. In this case, we plot the leading edge time versus the amplitude of all 511 keV shared events. Figure 6(b) shows the time distribution of the different time stamps corresponding to regions from I to III together with the overall distribution obtained by choosing all the events without any corrections. We proceed to fit each time distribution to a Gaussian and correct each value by the time resolution of the LSO:Ce:Ca co-doped reference crystal. The results are shown in figure 6(c), where we find the DTR for events fully contained in BGO and for the events sharing part of the 511 keV with the neighboring material with and without time walk correction.

The timing obtained for the different regions from I to III is shown without any time walk correction and indeed follows the expected trend with values ranging from 100 ps to 40 ps FWHM DTR. Applying a time-walk correction to all the events sharing 511 keV drive the timing down to 67 ps (equivalent CTR of 95 ps) which constitutes an improvement compared to the timing yielded by BGO events of 117 ps (equivalent CTR of 165 ps).

3.3. Timing with the LYSO + BC-422 sampling pixel

The second case study is very similar to the previous one with the only difference that BGO plates are now replaced by LYSO plates, same thickness. For this particular sampling pixel, the event identification using the signal rise time is slightly more challenging due to the fast emission characteristic of both LYSO and BC-422. Also the light output of LYSO is at least three times higher than BC-422, hence shared events will not appear shifted towards higher energies but in the opposite direction where Compton events are located. Shared 511 keV events in the 2D plot of integral versus amplitude will be always those going from the photopeak of the high-Z scintillator towards the Compton edge of the plastic BC-422. For the LYSO + BC-422 sampling pixel, since the light output of LYSO is higher than the light output of BC-422, the shared 511 keV will be placed towards smaller integrated charges values but higher amplitudes.

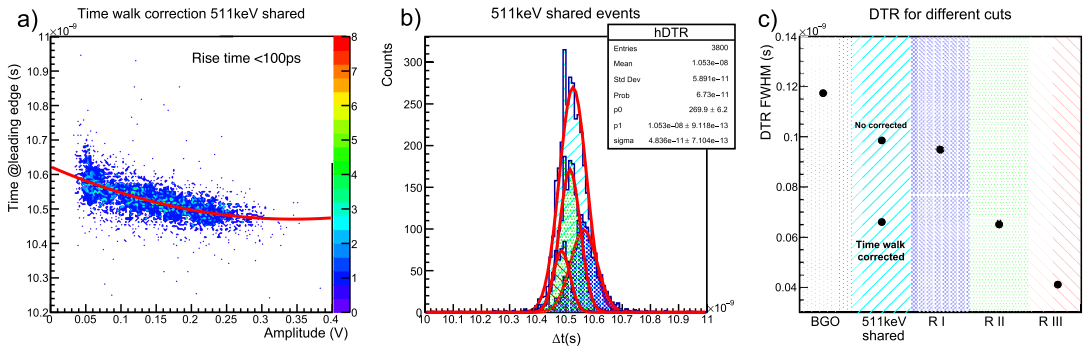

Figure 6. DTR measured with the BGO + BC-422 sampling pixel. (a) Time walk influence for all shared 511 keV events. (b) Time distributions for the different regions and all 511 keV shared events together. (c) Summary of the measured DTR values.

Figure 7(a) shows the rise time as function of the integral for all the coincidence events triggered. In this case, most of the events have a rise time smaller than 100 ps, however looking at the 2D correlation we are able to identify the Compton edge of BC-422 with an integral value of around 9nVs. LYSO 511 keV fully contained events can be seen with an integral value close to 20nVs. Events with an integrated charge in-between the Compton edge of plastic and the LYSO photopeak with a rise time of around 50 ps correspond to shared 511 keV events.

Due to the complex rise time cut that we would need to apply if we want to discard LYSO fully contained events, we proceed to do the DTR data analysis using just the information provided by the voltage amplifier. In this way, we are also able to test the feasibility of having just one extra parameter to calculate the DTR. Figure 7(b) shows the integral as a function of the signal amplitude for all the events as measured with the sampling pixel. We can identify all the events depositing some energy outside the LYSO by directly comparing to the figure 3(b) center, where we measured bulk LYSO:Ce. For this case, 511 keV shared events can be seen again between the BC-422 and LYSO characteristic lines and they occupy the space below the LYSO photopeak. As in the previous section, the regions I–III have been chosen in order to look into events with different energy distributions and they are labeled accordingly in figure 7(b). The plots shown along these contribution are 2D contour plots chosen to represent the more densely populated zones, therefore it might seems like region III has very few events, when in reality it is just a visual artifact coming from the fact that in this plot we include also 511 keV LYSO events.

The time resolution measured for the different types of events in the LYSO + BC-422 sampling pixel are shown in figure 8. The plot (a) contains the time distributions of the different regions together with the distribution of all 511 keV events, either shared or not. Figure 8(b) represents the time-walk corrected distribution for all the 511 keV shared events which yields a DTR value of 39 ps FWHM (equivalent CTR of 55 ps). A summary of all the measured DTR values for the different types of events is shown in figure 8(c). From left to right, we show the DTR of all 511 keV events together, labeled as 'All', the timing of 511 keV normal events, labeled as 'LYSO', the time walk corrected DTR of 511 keV shared events positioned in the shared column (Cyan stripes) and the DTR values for RI-III in the last three columns (blue and green dots, red stripes).

The standard timing, i.e. 511 keV fully contained in LYSO, is slightly deteriorated for the sampling case, going from 54 ps measured with the bulk material up to 57 ps ($CTR_{equiv} = 83$ ps). The improved timing for regions I–III is shown in the last three columns and it goes from 53 ps ($CTR_{equiv} = 75$ ps) for events with small energy leakage to the BC-422 down to 40 ps for events with medium and high energy leakage.

In this case, we observe a saturation for the DTR of the region III compared to the region II. Also, a DTR of 25 ps FWHM, which corresponds to the time resolution of bulk BC-422, is never reached, not even with events depositing energy only in plastic and centered at 340 keV. Thus, a deeper study of light transport within the BC-422 plates should be taken into account in future studies.

4. Discussion

In this contribution we have implemented a new concept to achieve faster time resolution for a fraction of the 511 keV events fully contained in a sampling pixel. A summary of the state-of-the-art DTR for the bulk scintillators and sampling pixels is shown in figure 9 as a function of the effective photon time density given by the light output and the scintillation kinematics. The pie charts included next to each sampling pixel represent the percentage of different types of events with respect to the total number of 511 keV gammas detected as obtained in the measurements. The classification of Compton events has been done by subtracting the events identified as 511 keV to the total number of events in coincidence. Events with total energy deposition in the sampling pixel are those placed after the Compton edge of the high-Z scintillator and they extend in a line, which reach out from

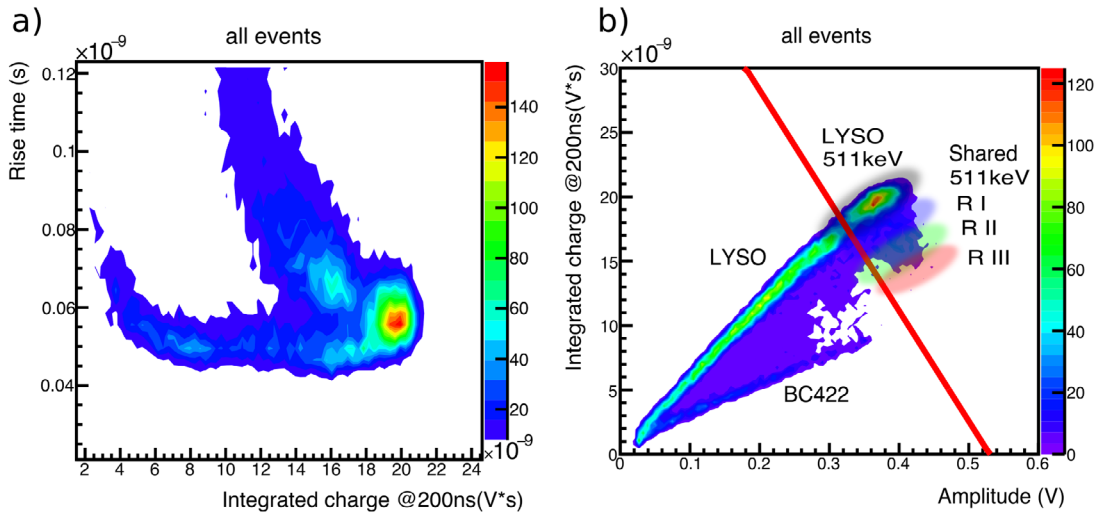

Figure 7. Event identification for the LYSO + BC-422 sampling pixel. (a) Rise time as function of the integral for all the events in coincidence. (b) Integral as a function of the amplitude for all the events in coincidence.

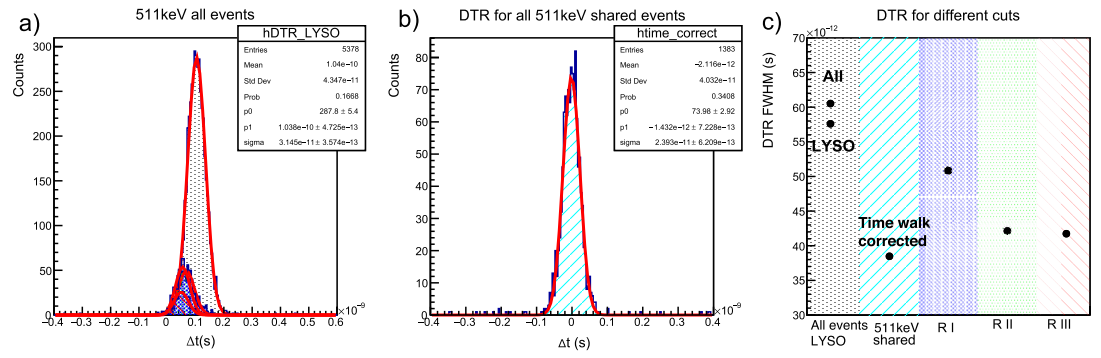

Figure 8. DTR measured with the LYSO + BC-422 sampling pixel. (a) Time distributions for the different regions and all 511 keV events together, fully contained in LYSO and shared. (b) Time distribution for all 511 keV shared events after time walk correction. (c) Summary of the measured DTR values.

the heavy scintillator photopeak towards the BC-422 Compton edge. For the case of BGO + BC-422, they are placed above the red line in figure 5(b) and for the LYSO + BC-422 pixel, they seat to the right of the red line in figure 7(b). All red lines were drawn from the Compton edge of the high-Z scintillator and parallel to the events with amplitudes or integrated charge higher than those characterizing the Compton edge of the plastic. Once the 511 keV events are identified, the only step done to separate shared from normal, is to subtract the events in the photopeak of the high-Z scintillator.

The timing reported for the sampling pixels is the one given by all 511 keV shared events after the time-walk correction (blue region in pie chart). The rest of 511 keV events (green region in pie chart) show up a timing slightly worse than the bulk case. We reach a DTR of 117 ps FWHM as compared to 112 ps for BGO and 57 ps as compared to 54 ps for LYSO. This is mostly due to a smaller light output of the plates ensemble.

It is interesting to notice that the timing achieved with 511 keV shared events for both sampling pixels is exactly the average of the DTR given by the individual scintillating components in their bulk shape. Also, the time-walk corrected timing of all 511 keV shared events yield values similar to the timing of region II, i.e. events sharing half of the energy in the heavy material and leaking out the other half. From that point of view, it seems logical that the improved timing of shared events could be easily estimated by averaging the timing given by the individual scintillating components when detecting 511 keV. This is one of the limitations of this method. If we choose to increase the photon time density by splitting the energy, the improved timing will never surpass the timing of the fast scintillator. However, for those fast emitting materials that are not capable of stopping or containing high energetic particles, this method offers a viable solution.

For the BGO + BC-422 case, if we compare the energy distribution obtained with simulated data (figure 4(a)) vs. measured data (pie chart in figure 9), we find results in very good agreement with discrepancy factors all ranging from 3%–7%. Compton events were predicted to represent around 57% of the detected gammas using

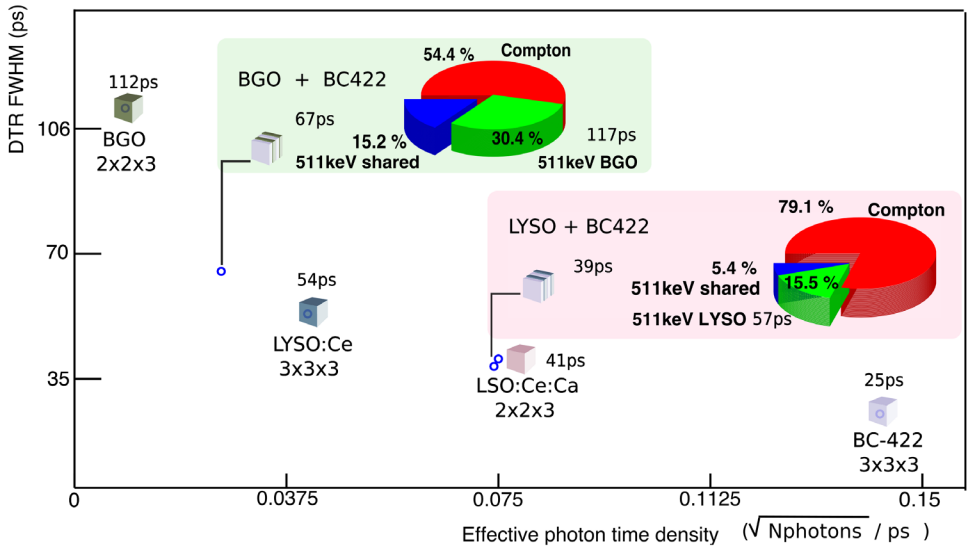

Figure 9. State-of-the-art DTR values measured for bulk scintillators and sampling pixels. DTR values represent shared events timing for the sampling case. The pie charts are representing the percentage of different type of events obtained with measured data.

Geant4 and the measurement yields around 54%. Also the percentage of shared 511 keV events with respect to the number of 511 keV events is in good agreement, around one third in both cases.

However, for the sampling pixel composed of LYSO + BC-422 the energy distribution measured is not as the one expected. Simulations for the LYSO sampling pixel predicts around 65% of the events will be Compton, 13% shared 511 keV and 22% 511 keV deposited in LYSO. In return, we get almost 80% of the events identified as Compton which is a factor 22% higher and this reflects in a ratio of 69% and 42% for the 511 keV normal and shared, respectively. We can think of two reasons for this disagreement. The first one related to the event identification in this sampling pixel, for which we do not apply a rise time cut and just use the 2D correlation between integral and amplitude. This can result in an overestimation of Compton events when they could be actually shared 511 keV events. Another factor would be the uncertainty related to the amount of plastic in the sampling pixel. BC-422 plates have been manually cut in our workshop and the thickness can be as high as 300 μm for some plates. In this regard, a more precise composition of the sampling pixel should be pursued in the future.

As explained in the previous section, measurements were taken for different leading edge thresholds, starting at 1mV up to nearly 100 mV. For the specific case of the BGO + BC-422 sampling pixel, we expected a very distinctive behavior when plotting the DTR as a function of the leading edge threshold for the two category of 511 keV events: 1. fully contained in BGO and 2. shared between BGO and BC-422. The timing for events fully contained in BGO is given by Cherenkov photons, hence the minimum DTR should be reached at very low thresholds. On the other hand, the timing of shared 511 keV events is mostly given by the BC-422 photons, therefore a stable DTR should be observed as a function of the threshold. These two features behave as foreseen and they are shown in figure 10. A minimum DTR for 511 keV fully deposited in BGO, i.e. standard timing, is reached for 8 mV threshold, however a minimum DTR of 57 ps is found all across the threshold scan for 511 keV events able to share energy, i.e. improved timing. This is important in view of building a highly integrated detector system, as good timing achievable with higher thresholds relaxes the requirements on the photodetector and electronic readout.

The method proposed in this contribution to improve the timing resolution for a fraction of the events intervenes with the homogeneity of the scintillating pixel. Therefore, its implementation needs a fine-tuning of the relevant factors such as stopping power, overall CTR performance and energy resolution. For this study we have chosen around 200 μm as a good enough sampling thickness, allowing to observe the different category of events. However, this number is not offering the best distribution of the 511 keV energy and an optimization can be found by decreasing the thickness of the plates and using a denser fast material. Simulations performed with different types of fast materials having a density up to 3 g cm^{-3} confirm that the loss in number of detected events in a sampling pixel could be decreased to a 10% in comparison to the homogeneous case. Regarding the distribution of 511 keV gammas, having the less dense material with a density up to 3 g cm^{-3} and a thickness of 100 μm, allows for the majority of the events to be fully contained and also to be shared. In this way, the events with normal time resolution could represent the 20% of the 511 keV events fully deposited, instead of 66% as presented here.

Regarding energy resolution, this value would not change for 511 keV normal events. However, for shared 511 keV events, a correction along the line of events with full energy deposition needs to be applied. Unless, we manage to align the channel of the Compton edge or photopeak for both materials, i.e. same light output within a given integration gate. In this particular case the line defining 511 keV shared events will be parallel to the

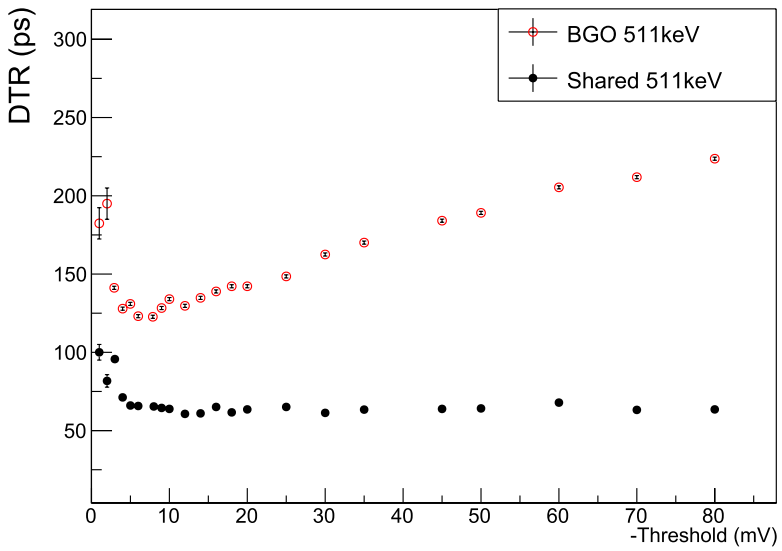

Figure 10. DTR for 511 keV events fully contained in BGO (red open dots) and 511 keV shared events (black solid dots) as a function of the leading edge threshold. (Time walk correction applied).

amplitude *x*-axis in the 2D correlation plot, which implies that no correction is needed. Promising configurations among different materials will be a topic to investigate in future publications.

The modest timing values obtained in this first study are an experimental proof that improvement can be found in a sampling configuration. This approach is at the center of our vision on how to tackle the 10 ps TOF-PET challenge and constitutes one of the first steps towards the implementation of nanocomposite scintillating layers in combination with high-Z inorganic materials. The complications regarding assembly and fabrication of sampling pixels are indeed a factor to take into account. However, the possibility of achieving real-time molecular imaging for cancer diagnosis deserves well dedicated efforts along this line of research.

5. Conclusions

In this contribution we were able to demonstrate that sampling a homogeneous pixel and including fast emitting materials in-between, bears significant potential as a solution to achieve ultra-fast timing with modest energies.

In the new detector configuration, we identified three main types of events: 1. Compton events not used for timing, 2. standard 511 keV events completely contained in the heavy scintillator and offering standard timing and 3. shared 511 keV events depositing energy in both materials and yielding improved timing.

We measure a time resolution of 67 ps DTR FWHM ($CTR_{equiv} = 95$ ps) for one third of the events depositing 511 keV in the BGO + BC-422 sampling pixel. The other two third of the 511 keV events perform as good as BGO by itself with a time resolution of around 117 ps ($CTR_{equiv} = 165$ ps) mediated by Cherenkov photons and the high frequency readout (Gundacker *et al* 2019). For the case of LYSO + BC-422 sampling pixel, shared 511 keV events reach a DTR of 39 ps ($CTR_{equiv} = 55$ ps) in comparison to 57 ps ($CTR_{equiv} = 83$ ps) for 511 keV events fully contained in LYSO.

This is a first attempt to understand how to exploit energy sharing in order to improve timing resolution on a fraction of the events with a very simple geometry. This fraction can be increased with optimized configurations of the two types of scintillators by reducing the sampling thickness and increasing the density of the fast emitting material.

The use of new unconventional materials, not suitable by themselves for PET applications, can now be considered in a sampling detector configuration that uses two scintillators. The possibility of measuring the time resolution with 511 keV using materials not able to contain such amount of energy opens the door and would contribute to the development of nanoscintillators and multiple quantum well heterostructures for radiation detector applications.

Acknowledgment

This research has been supported by the ERC Advanced Grant no. 338953 (TICAL, P I Paul Lecoq) and carried out in the frame of Crystal Clear collaboration, COST Action TD1401 and the ASCIMAT project under grant agreement 690599. The authors would like to express their gratitude to Dominique Deyrail from CERN EP-CMX-DA for the preparation of the BC-422 tiles.

ORCID iDs

R M Turtos https://orcid.org/0000-0002-1077-4849
S Gundacker https://orcid.org/0000-0003-2087-3266

References

Bulin A L, Vasil'ev A, Belsky A, Amans D, Ledoux G and Dujardin C 2015 Modelling energy deposition in nanoscintillators to predict the efficiency of the x-ray-induced photodynamic effect *Nanoscale* **7** 5744–51

Grim J Q, Christodoulou S, Stasio F D, Krahne R, Cingolani R, Manna L and Moreels I 2014 Continuous-wave biexciton lasing at room temperature using solution-processed quantum wells *Nat. Nanotechnol.* **9** 891–5

Gundacker S, Acerbi F, Auffray E, Ferri A, Gola A, Nemallapudi M, Paternoster G, Piemonte C and Lecoq P 2016a State of the art timing in TOF-PET detectors with LuAG, GAGG and L(Y)SO scintillators of various sizes coupled to FBK-SiPMs *J. Instrum.* **11** P08008

Gundacker S, Auffray E, Pauwels K and Lecoq P 2016b Measurement of intrinsic rise times for various L(Y)SO and LuAG scintillators with a general study of prompt photons to achieve 10 ps in TOF-PET *Phys. Med. Biol.* **61** 2802

Gundacker S, Turtos R M, Auffray E, Paganoni M and Lecoq P 2019 High-frequency SiPM readout advances measured coincidence time resolution limits in TOF-PET *Phys. Med. Biol.* **64** 055012

Hospodková A, Hubáček T, Oswald J, Pangrác J, Kuldová K, Hývl M, Dominec F, Ledoux G and Dujardin C 2017 InGaN/GaN structures: effect of the quantum well number on the cathodoluminescent properties *Physica Status Solidi* b **255** 1700464

Kharchenko V and Rosen M 1996 Auger relaxation processes in semiconductor nanocrystals and quantum wells *J. Lumin.* **70** 158–69 (Spectroscopy of isolated and assembled semiconductor nanocrystals)

Klimov V I 2014 Multicarrier interactions in semiconductor nanocrystals in relation to the phenomena of auger recombination and carrier multiplication *Ann. Rev. Condens. Matter Phys.* **5** 285–316

Lecoq P 2017 Pushing the limits in time-of-flight PET imaging *IEEE Trans. Radiat. Plasma Med. Sci.* **1** 473–85

Padilha L A, Bae W K, Klimov V I, Pietryga J M and Schaller R D 2013 Response of semiconductor nanocrystals to extremely energetic excitation *Nano Lett.* **13** 925–32

Saint-Gobain 2016 Premium plastic scintillators (www.crystals.saint-gobain.com/sites/imdf.crystals.com/files/documents/bc418-420-422-data-sheet.pdf)

Turtos R M, Gundacker S, Lucchini M T, Procházková L, Čuba V, Burešová H, Mrázek J, Nikl M, Lecoq P and Auffray E 2016a Timing performance of ZnO:Ga nanopowder composite scintillators *Physica Status Solidi* **10** 843–7

Turtos R M, Gundacker S, Pizzichemi M, Ghezzi A, Pauwels K, Auffray E, Lecoq P and Paganoni M 2016b Measurement of LYSO intrinsic light yield using electron excitation *IEEE Trans. Nucl. Sci.* **63** 475–9

Turtos R M, Gundacker S, Polovitsyn A, Christodoulou S, Salomoni M, Auffray E, Moreels I, Lecoq P and Grim J 2016c Ultrafast emission from colloidal nanocrystals under pulsed x-ray excitation *J. Instrum.* **11** P10015

Wilkinson J, Ucer K and Williams R 2004 Picosecond excitonic luminescence in ZnO and other wide-gap semiconductors *Radiat. Meas.* **38** 501–5 (*Proc. of the 5th European Conf. on Luminescent Detectors and Transformers of Ionizing Radiation (LUMDETR 2003)*)